1-2-2018

Algorithm Development for Intrafraction Radiotherapy Beam Edge Verification from Cherenkov Imaging.

Clare Snyder
Dartmouth College

Brian W. Pogue
Dartmouth College

Michael Jermyn
Dartmouth College

Irwin Tendler
Dartmouth College

Recommended Citation
Snyder, Clare; Pogue, Brian W.; Jermyn, Michael; and Tendler, Irwin, "Algorithm Development for Intrafraction Radiotherapy Beam Edge Verification from Cherenkov Imaging," J. Med. Imag., 5(1), 015001, (2018); doi: 10.1117/1.JMI.5.1.015001

Journal of Medical Imaging

MedicalImaging.SPIEDigitalLibrary.org

Algorithm development for intrafraction radiotherapy beam edge verification from Cherenkov imaging

Clare Snyder
Brian W. Pogue
Michael Jermyn
Irwin Tendler
Jacqueline M. Andreozzi
Petr Bruza
Venkat Krishnaswamy
David J. Gladstone
Lesley A. Jarvis

Clare Snyder, Brian W. Pogue, Michael Jermyn, Irwin Tendler, Jacqueline M. Andreozzi, Petr Bruza, Venkat Krishnaswamy, David J. Gladstone, Lesley A. Jarvis, "Algorithm development for intrafraction radiotherapy beam edge verification from Cherenkov imaging," *J. Med. Imag.* **5**(1), 015001 (2018), doi: 10.1117/1.JMI.5.1.015001.

Journal of Medical Imaging 5(1), 015001 (Jan–Mar 2018)

Algorithm development for intrafraction radiotherapy beam edge verification from Cherenkov imaging

Clare Snyder,[a] Brian W. Pogue,[a,b,c,*] Michael Jermyn,[a,b] Irwin Tendler,[a] Jacqueline M. Andreozzi,[a] Petr Bruza,[a] Venkat Krishnaswamy,[a,b] David J. Gladstone,[a,c,d] and Lesley A. Jarvis[c,d]
[a]Dartmouth College, Thayer School of Engineering, Hanover, New Hampshire, United States
[b]DoseOptics LLC, Lebanon, New Hampshire, United States
[c]Dartmouth–Hitchcock Medical Center, Norris Cotton Cancer Center, Lebanon, New Hampshire, United States
[d]Geisel School of Medicine, Department of Medicine, Hanover, New Hampshire, United States

Abstract. Imaging of Cherenkov light emission from patient tissue during fractionated radiotherapy has been shown to be a possible way to visualize beam delivery in real time. If this tool is advanced as a delivery verification methodology, then a sequence of image processing steps must be established to maximize accurate recovery of beam edges. This was analyzed and developed here, focusing on the noise characteristics and representative images from both phantoms and patients undergoing whole breast radiotherapy. The processing included temporally integrating video data into a single, composite summary image at each control point. Each image stack was also median filtered for denoising and ultimately thresholded into a binary image, and morphologic small hole removal was used. These processed images were used for day-to-day comparison computation, and either the Dice coefficient or the mean distance to conformity values can be used to analyze them. Systematic position shifts of the phantom up to 5 mm approached the observed variation values of the patient data. This processing algorithm can be used to analyze the variations seen in patients being treated concurrently with daily Cherenkov imaging to quantify the day-to-day disparities in delivery as a quality audit system for position/beam verification. [DOI: 10.1117/1.JMI.5.1.015001]

Keywords: radiation therapy; dosimetry; quality audit; image processing; linac.

Paper 17299R received Sep. 30, 2017; accepted for publication Dec. 5, 2017; published online Jan. 2, 2018.

1 Introduction

Radiation therapy treatment verification is always needed for independent systems that report on a combination of factors involved such as beam position and patient position throughout beam delivery. From recent data on incident learning, it is suggested that human factors of daily fractionation in a busy department could benefit from verification that is more implicit, requiring less active involvement.[1–3] An "always on" approach to checking set up and delivery would be beneficial both for time saving, as well as reducing delivery error incidents, given that most incidents would be detected during the delivery process.[4] In this study, the concept of Cherenkov imaging, as shown in Fig. 1, is examined as a verification tool, specifically focusing on the capabilities of what could be done with the surface delivery images that are provided by such a system. The workflow for image processing and analysis, which forms a backbone of an automated detection system was developed and analyzed.

Daily verification of intensity-modulated radiation therapy is based upon electronic portal imaging dosimetry recording of the entire treatment delivery and this can be used for transit dosimetry where the portal imaging is used for computational estimation of what dose was delivered to the volume.[5] This process has evolved to the point where it is sufficiently accurate and has been widely adopted to replace the more labor-intensive use of port films.[6] Early trials indicated sufficient clinical acceptance criteria within 7% intensity variation criteria for matching the measured dose to the plan.[5] However, the factor that tends to limit portal dosimetry-based verification is the question of whether daily verification is really necessary, versus weekly or not at all,[7] given the time constraints and the small likelihood of detecting an incident that is not detectable in other aspects of the quality controls already in place.[8] While the acquisition can be automated, the bulk of the concern comes from time required in analysis, given that this piece of the verification process is not automated. Also, there remain small concerns about a couch or patient collision with the EPID detector in cases where the patient couch is moved. A system that implicitly mapped the patient position and treatment delivery with automated verification of day-to-day repeatability is inherently possible with sufficient input to the engineering design.

Surface patient position mapping has developed to the point where verification of position of the body on the couch can be reliably assessed with very little input, and the mapping comparison to each day is fully automated. The feature of these systems that make them ideal verification tools is that they employ optical imaging, implicitly doing all measurements from the ceiling, out of the way of the therapist users, and with online software that does the comparison without need for active participation of the therapy team. Cherenkov imaging of radiation therapy dose delivery is an additional feature possible with optical imaging; it has been shown to map the radiotherapy beam on the patient's tissue[9,10] while being a passive optical imaging system, out of the way of the therapist. Analysis of Cherenkov images could be as automated as the currently adopted optical

*Address all correspondence to: Brian W. Pogue, E-mail: brian.w.pogue@dartmouth.edu

2329-4302/2018/$25.00 © 2018 SPIE

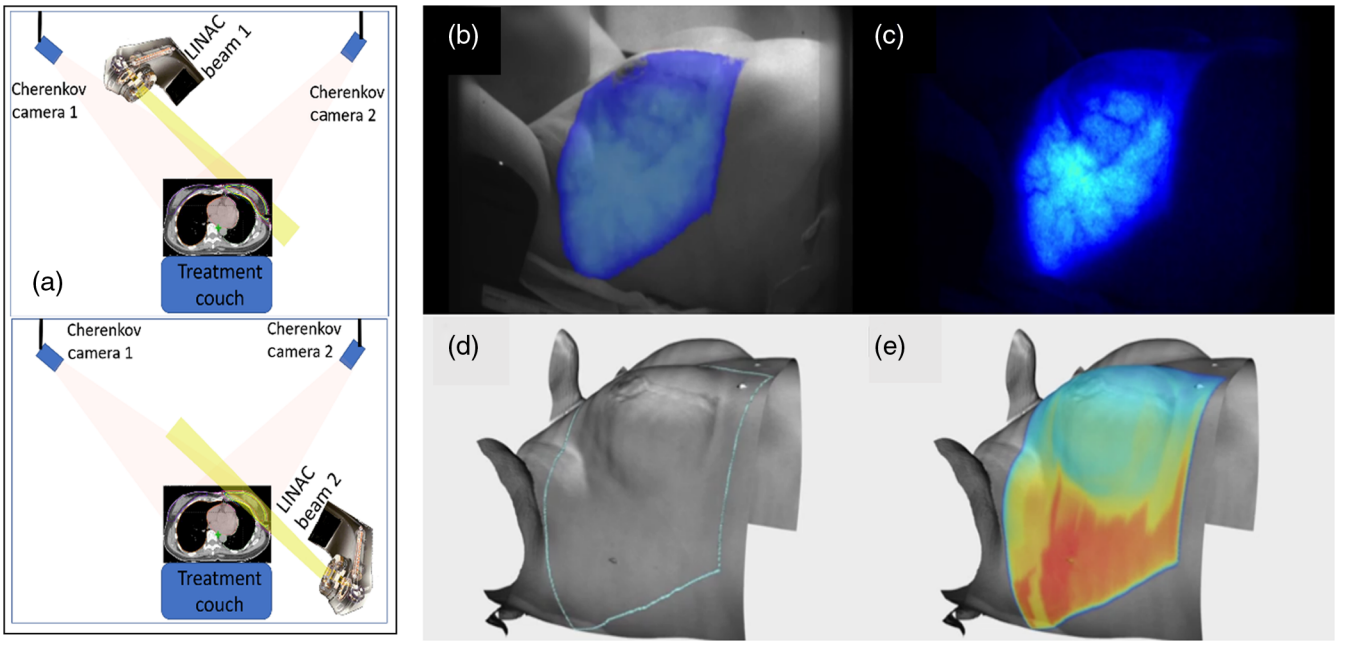

Fig. 1 (a) Images of the Cherenkov imaging geometry used with the cameras mounted on the ceiling, to image the two tangential beams for whole breast irradiation (top and bottom). Real-time Cherenkov light imaging during whole breast radiation therapy is shown (b), overlaid on the image of the patient. (c) Cumulative Cherenkov image without the overlay. (d) The prescribed treatment area is outlined in blue, based on the configuration of the gantry, multileaf collimator, and beam. (e) Planned surface dose extracted from the top 5 mm of tissue.

patient mapping systems,[11] but the unique features of these images must be dealt with appropriately. This aspect of a verification approach is the subject of this study.

Cherenkov images are captured from the low light emission from secondary electrons in patient tissue during therapy,[12] and time-gating of the detection has been the key to capturing this very low light signal within an ambient room light background.[13,14] These images are formed from relatively few photons captured by the camera, with most estimates being near about 10 to 20 photons per pixel. Thus, the images are highly noisy and relatively low in feature space. Yet, for verification it would be desirable to be able to delineate the beam edges on the image, relative to the body position.[11] The workflow for how to map out the beam edges with maximal accuracy was the primary focus of this study, with the goal of being able to have an automated algorithm that could pick out day-to-day variations of intrafraction treatment.

2 Materials and Methods

2.1 *Cherenkov Imaging*

In the radiotherapy unit at the Dartmouth–Hitchcock Medical Center, a CDose Cherenkov imaging camera (DoseOptics LLC, Lebanon, New Hampshire) was installed in the ceiling of the room, at a fixed location. The camera was running at 20 frames per second, with the linac pulsing at ~360 Hz, leading to 18 pulses per read out frame. The spatial resolution of these images was ~1 mm and the readout was a 2-D image which was 1920×1200 pixels, leading to a pixel dimension size of 0.3-mm square.

Breast irradiation was completed with a standard set of two tangential beam angles at 6 MV for all these subjects, having at least three control points for each patient; here a control point describes a single planned configuration of the beam-shaping multileaf collimator. Three control points were analyzed per patient. Most of the treatment dose was delivered in the first broad beam control point, and then the latter two (or more) were shaped beams delivering more dose to the chest wall, as shown in the top box of Fig. 2.

To analyze the total delivered dose at each control point, the video sequences of Cherenkov images were processed in two stages. First each stack of images from the video sequence was temporally median filtered over five sequential images within each control point, and then these images were spatially median filtered in a 5×5 kernel. Then the resulting set of temporal images was summed throughout that control point to create a total single image of the total Cherenkov recorded during that period of time. The choice of a 5×5 spatial median filter was selected based upon previous studies, which appeared to suppress hot pixel noise well but not degrade spatial resolution of the images too much. Each patient was imaged up to nine individual daily fractions, to assess the image changes over this span of time.

2.2 *Noise Suppression Image Processing*

All image analysis was prototyped using the MATLAB image processing toolbox (Mathworks Inc., Natick, Massachusetts). The accumulated control point images (top box in Fig. 2) were completed for each daily fraction (second box from the top). These images were then used for noise processing and analysis. Since the patient images were composed of relatively high noise data, it was desired to suppress some of the noise (box 3) before feature extraction (box 4).

The choice of the denoising method was affected by the need to keep sharp image features, with particular focus on

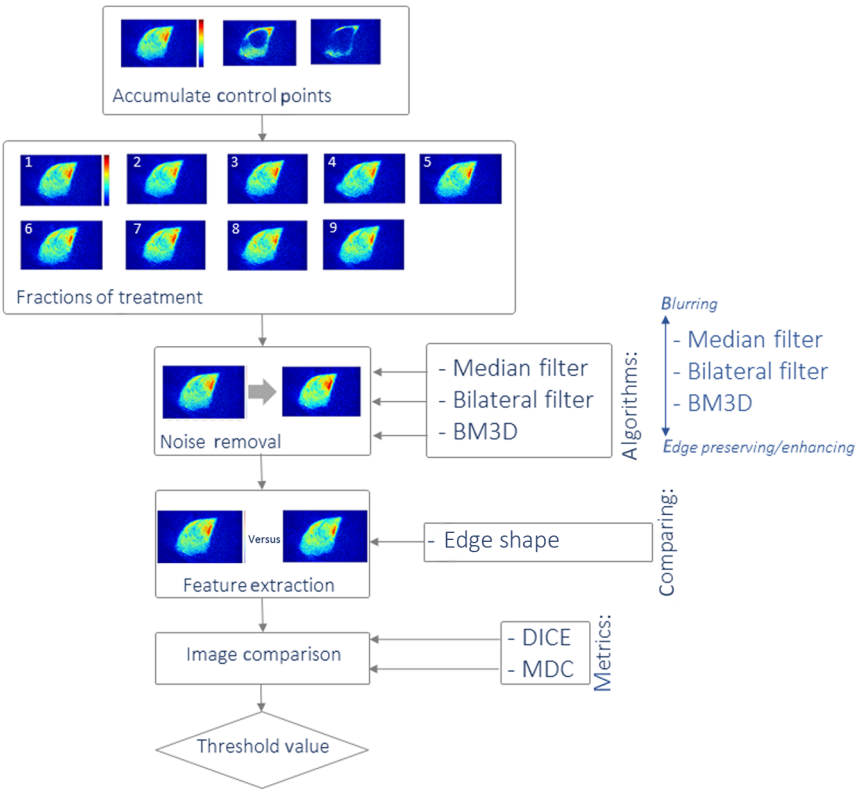

Fig. 2 Illustration of the analysis process being examined is shown as a flowchart with optional image processes coming in from the right.

maintaining high spatial frequency in the beam edges. As shown in a previous study,[11] several features could be extracted, including internal image features related to the beam and patient tissue, such as blood vessels. However, in this study, the choice was made to focus initially on the beam shape at each control point as a verification tool. In the case of the composite Cherenkov images, blurring the beam edge would change the perceived shape of the beam, and in turn, lessen the accuracy of image comparisons. Therefore, it was important to choose an edge-preserving filtering method. The three methods chosen here had this property, including: median filtering, bilateral filtering,[15] and block-matching and 3-D filtering (BM3D) (inputs to box 3). The median filtering suppresses features that are well outside the inner quartile ranges of the intensity values, and the bilateral filter also does this but preserves the ability to have a step function change in intensity. Finally, the block-matching with 3-D filtering groups similar 2-D patches in images into a 3-D block, and uses 3-D filtering to denoise the images. These were studied for their effects upon the images and the extractions.

2.3 *Phantom Imaging*

To compare the processed images to a quantitatively known set of images, which were known to be either in the exact same position or to have been moved by well-known distances, a series of phantom studies was carried out. All phantom data were collected with a set of radiation treatment plans with a single fixed camera setup. A breast phantom ($24 \times 18 \times 12$ cm) was milled from off-white ABS plastic (Proto Labs, Inc., Minnesota). The shape of the breast surface was generated from a CT of a breast patient. To simulate light attenuation by blood filled veins, a 4-mm-wide Kapton tape was attached on the top surface in a vein-like pattern. The material was chosen because it demonstrated similar levels for Cherenkov emission to human tissues, as shown in Fig. 3.

Imaging was carried out for five different treatment plans with varying levels of beam modulation. First, two tangent fields with opposing gantry angles were imaged with a standard, open field similar to the first control point of a clinical patient plan. Second, the two tangent fields were again imaged, but with an applied dynamic wedge. The dynamic wedge uses the photon jaw to continuously shrink the field size from an open to closed position in one direction, making wedge intensity over time when the frames are integrated, simulating a static wedge, which could be present physically. Finally, a treatment beam most analogous to a clinical patient treatment plan was imaged, where the multileaf collimator (MLC) shaped the beam to six control points. Just as in the patient imaging, each control point is an MLC segment with an expected unique beam shape on the phantom.

Five repeated imaging sessions were administered with no movement throughout treatment, to determine the baseline variation in the images for minute fluctuations within the treatment beams and the camera readout. The static variation images were processed in the same way as the clinical images. Following this, the phantom was shifted in well-known distances, and each plan was retreated five times with full imaging. This was repeated for each of three moved positions of the phantom, designed to be: (a) 1.0 mm, (b) 3.0 mm, and (c) 5.0 mm from original position, in the AP direction, using the accurate translation of the treatment couch. Again, the same control point integrated images were developed for each of these 100

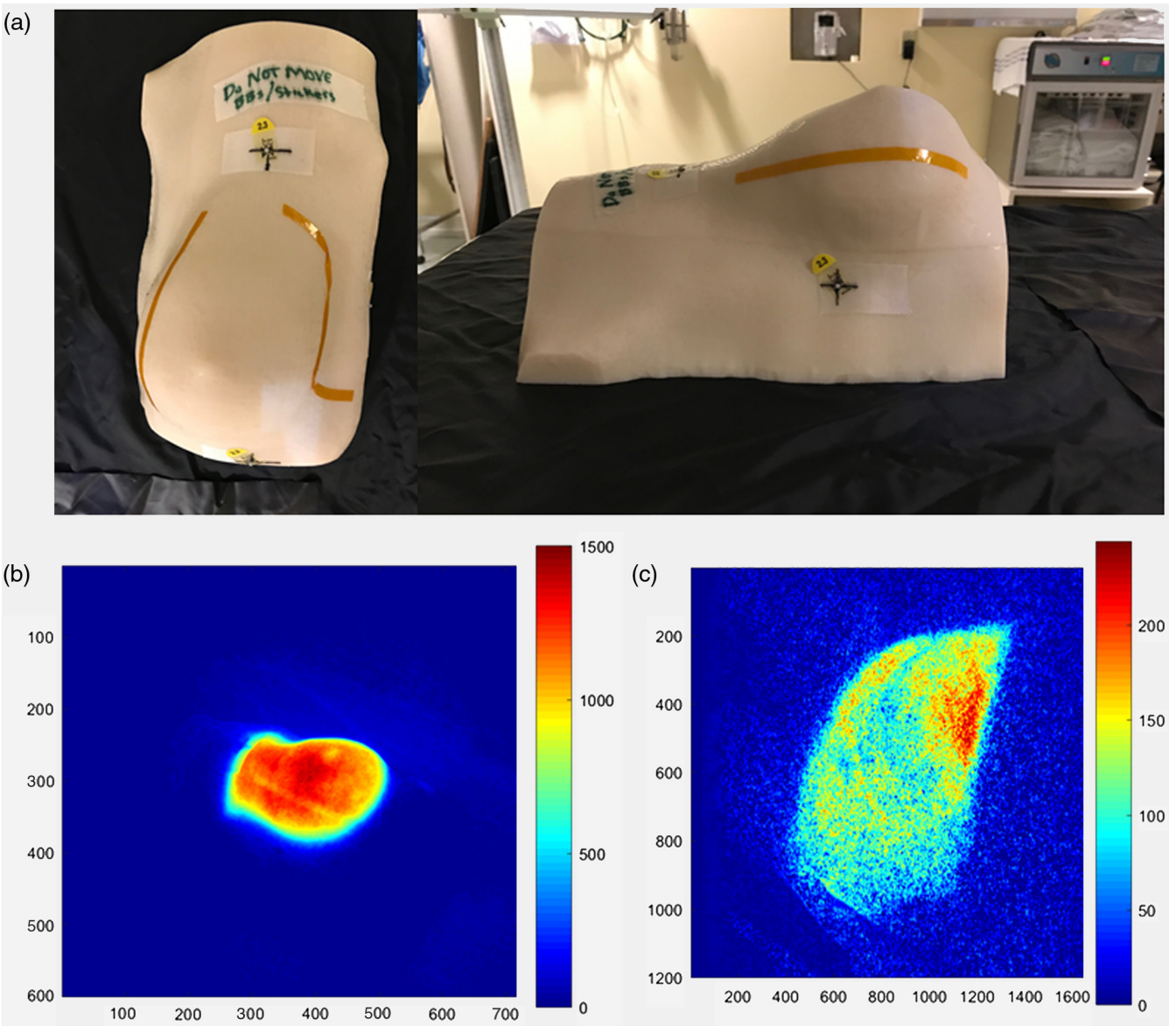

Fig. 3 (a) Breast phantom created from a true breast mold is shown with fiducials and tape lines to simulate blood vessels in the images, (b) right-sided perspective of the breast phantom, and (c) Cherenkov composite image as recorded during a radiotherapy treatment.

sets of images (five treatment beams × five iterations × four phantom positions). These well-controlled single direction movements were used to assess the changes to the images for well-characterized shifts. The images were shifted only in the AP direction, which is equivalent to shifting in the PA direction given reciprocity. This controlled linear shift was specifically chosen to allow analysis of well-controlled and well-understood position variations.

2.4 *Patient Imaging*

All imaging sessions were completed within compliance of an ongoing clinical study, which was approved by the Institutional Review Board of the Trustees of Dartmouth College. The patients were admitted into the study after providing informed consent to participate in this imaging study. All treatments and imaging were completed within the Radiation Oncology Program of the Norris Cotton Cancer Center at the Dartmouth–Hitchcock Medical Center, following standard radiotherapy treatment protocols.

The room used for all patients housed a Varian Clinic 2100CD (Varian Medical Systems, Palo Alto, California) providing 6- and 10-MV photon beams for whole breast radiotherapy. A total of seven patients' images were used for this study. Imaging of each subject as described above included their entire treatment plan with continuous acquisition throughout all control points.

2.5 *Image Feature Extraction*

The comparison of daily intrafraction treatments requires a reference image with which to associate each day's beam. The reference images for each patient were created by averaging the binary Cherenkov images from each patient and binarizing

this image. This approach was chosen to mimic what seemed a reasonable way to compare images from subsequent imaging sessions. For each phantom treatment beam, a reference image was made using the same process, but with the average of only the binary images of the beam at its original position (moved 0 mm), not of binary images at all positions. These reference images were then thresholded with the same value as all other images, and the resultant compared with each binary image from that same control point, from the corresponding patient or phantom. Two metrics were used to provide quantitative comparisons, the Dice coefficient and mean distance to conformity (MDC).

The Dice coefficient is a very commonly used metric within medical imaging, and is calculated as

$$\text{Dice coefficient} = \frac{2|A \cap B|}{|A| \cup |B|},$$

where the output coefficient has a value between 0 and 1, where 1 indicates complete overlap between the images and 0 is no overlap. A and B are the binary images being compared, after they had been thresholded at the same values, and $|x|$ is the nonzero volume of x. $A \cap B$ is the overlap of nonzero pixels between A and B.

The MDC value represents the average distance in millimeters that the perimeter of the binary image must move to conform to the perimeter of the reference image. Here, an MDC value of 0 would indicate a perfect match between two binary images, while larger MDC values show poor matches among images. The MDC was calculated as

$$\text{MDC} = \sum_{p \in A \cap !B} d(p, B) + \sum_{p \in !A \cap B} d(p, A),$$

where A and B are the binary threshold masks being compared, d provides the minimum distance between a pixel p and a mask. For every pixel in either A or B exclusively (not both), the minimum distance of the pixel from the other mask is accumulated. Each of these was calculated on all phantom and human images, and the results of these calculations are visualized graphically to allow comparison between the phantom and human data values.

3 Results

3.1 *Noise Suppression*

The noise processing algorithm choices needed to be determined first, because as shown in the flowchart of Fig. 2, this would potentially impact feature extraction and the ultimate results of intrafraction comparisons. As shown in Fig. 4, the filtering methods chosen for analysis were all edge-preserving. The raw image is shown in (a) and the filtered versions for BM3D, median, and bilateral were all tested, with representative versions shown in (b) through (d).

The parameters for these filtered images were chosen based upon minimization of variation between subsequent processed images; the parameters were large enough to remove most noise while preserving the features of the image, thereby reducing frame to frame "noise." The sigma value used in BM3D filtering was set to 100, based upon successive trials to minimize difference among images. Images were also spatially processed over a 5×5 pixel kernel and temporally filtered over five sequential images, based upon previous work, and while this was less quantitative, it was found to be the minimum size kernel to suppress hot pixels. Default values were used for bilateral filtering based upon the algorithm supplied,[15] with "box bilateral filtering" being chosen over "Gaussian bilateral filtering" for its edge-preserving characteristics, and preservation of the high-frequency content needed for edge detection, despite having similar filtering of the noise. The input sigma parameter values in the algorithm were varied over a fairly wide range, but the resulting output images were found to be largely similar independent of the choice of parameters, as long as it was in the range of 10 to 70.

The difference images between the filtered and the raw are shown for each of the filtered images immediately below them in (e) through (g), respectively. After comparing a range of images, with representative images as shown in Fig. 4, median filtering was ultimately chosen for its ease of use and quality of resulting images. The value of the filters is apparent from the

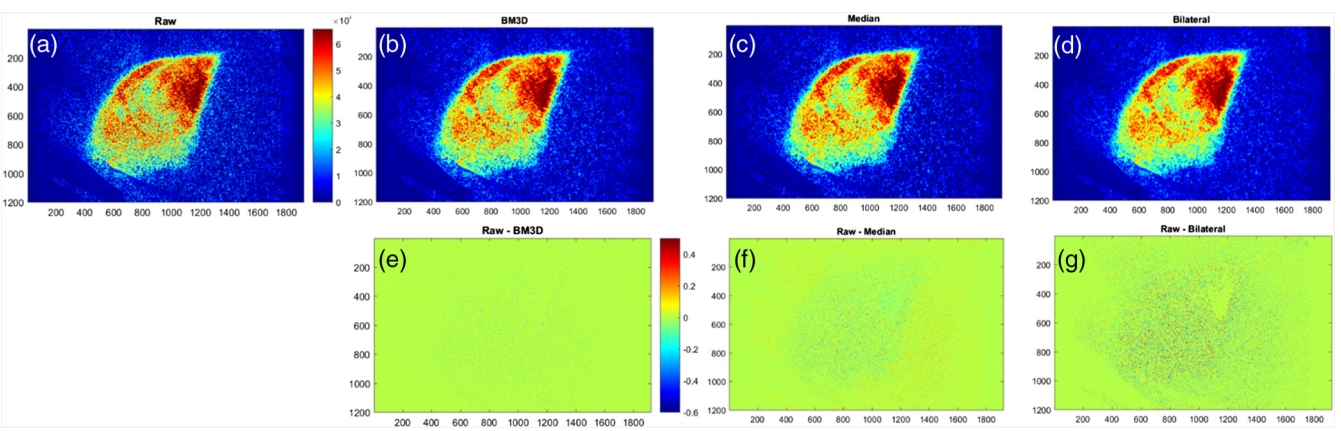

Fig. 4 Filtering methods: (a) unfiltered Cherenkov composite image, (b) BM3D filtered image, (c) median filtered image, (d) bilateral filtered image, (e) BM3D filtered image subtracted from unfiltered image, (f) median filtered image subtracted from unfiltered image, and (g) bilateral filtered image subtracted from unfiltered image.

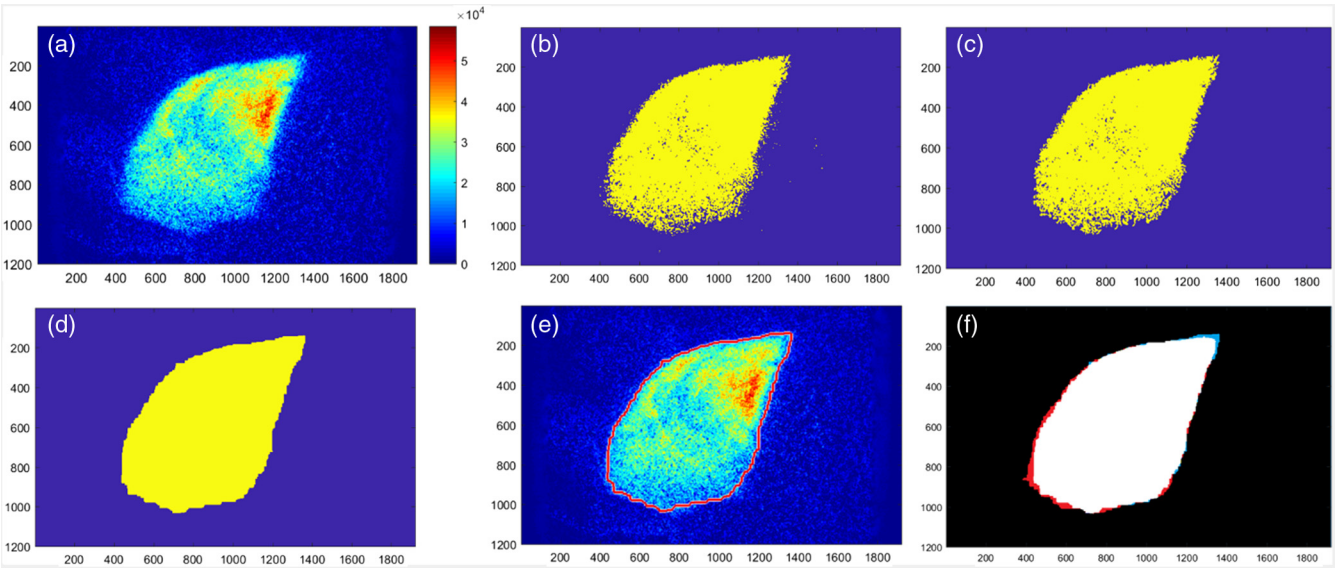

Fig. 5 The binarization process is outlined as: (a) Cherenkov composite patient image from the first day, (b) binarized Cherenkov image, (c) denoised binarized image, (d) morphologically closed holes in the binary image, (e) Cherenkov image overlaid with the perimeter of the binary image (in red), and (f) overlap of the patient binary image with the binarized average of all patient binary images (for this subject). White indicates overlap, black indicates the background, red indicates the binarized average, and blue indicates the day one binary image.

differences images below them (e) to (g), where more residual throughout the images indicates lost information.

3.2 *Thresholding*

The beam edges were isolated by binarizing the filtered, composite Cherenkov images. The threshold for this binarization was found using the Otsu's method and a 256-bin image histogram [Fig. 5(b)]. The noise in the binary images, defined as being any nonzero region < 400 pixels, was then removed [Fig. 5(c)]. To remove any remaining holes in the binary beam images, images were morphologically closed with a 100-pixel $\times$ 100-pixel structuring element neighborhood [Fig. 5(d)] using MATLAB dilation followed by erosion. The 100×100 structuring element defines the area of the holes that are closed. This area was chosen for being the size that certainly removes all holes caused by noise, which always falls within this area, while still being too small to distort or smooth the edges of the binary images. The values used in this binarization process were chosen for producing binary images that most closely matched the perimeter of the beam in the Cherenkov composites [Fig. 5(e)], where the similarity of the match was determined by comparison as shown in Fig. 5(f).

3.3 *Phantom Analysis*

To understand how beam similarity changed with distance, the Dice coefficient and MDC values were calculated for all 100 phantom treatments, relative to their averaged value. Figure 6 shows these values and illustrates the change in value for each distance. The breast phantom was completely stationary in the first instance (left most data), not being moved among images taken at the same distance from the camera. Thus, this image set served as a control to show only the variation in the radiation pattern and camera readout. With no variation due to breathing, slight movement during treatment nor movement between beams, this set produced very high DICE coefficints of 0.990 and above and MDC coefficients of 1.0 to 1.75.

Next, the phantom images were acquired with systematically shifted positions of 1, 3, and 5 mm to analyze how the images would compare with known shift values in a very controlled setting. Each set of these values is plotted in Fig. 6 separated by clustering into colored region bars on the graph.

3.4 *Patient Image Analysis*

As with the phantom datasets, the Dice coefficients and MDC values were calculated for all patient treatments as shown in Fig. 7. The minimum values of the phantoms are also depicted on this graph by solid colored lines with corresponding shading used for clarity of display on the graph. This combination plot illustrates the results of these comparisons for the fractions of each patient, intended to provide a visualization of the misalignment implication of each quantitative patient Dice coefficient value with respect to the well-known phantom displacement data as shown in Fig. 7(a). Each line represents the minimum Dice coefficient for the labelled distance from the origin, with gradient shading on the graph to help visualize the range. Patient data all fall largely within the range of 5-mm shift Dice coefficient values execpt in 11 of the 100 treatments.

The MDC values for each fraction, in Fig. 7(b), show that the distances to conformity range between 1 and 4 mm. These are perhaps more absolute than the Dice values and match the setup expected for the patients while undergoing their fractionated treatments. Of the 69 phantom images, only 12 have Dice coefficients below 0.97, the lowest average Dice coefficient of the phantoms is at 5 mm from the origin.

4 Discussion

Cherenkov imaging has only recently been demonstrated during radiotherapy,[9] but the paradigm of using this imaging tool to

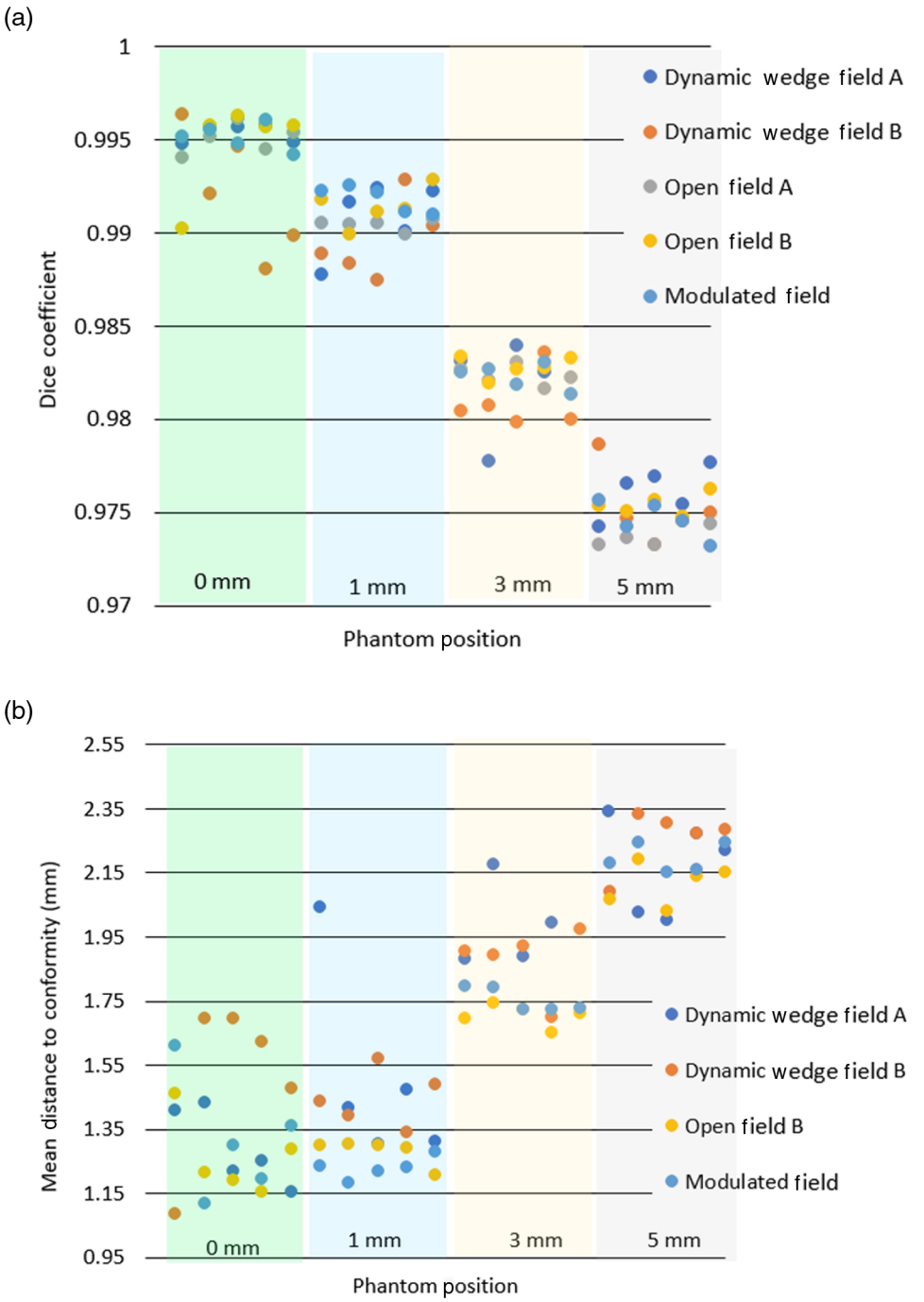

Fig. 6 Illustrates the (a) Dice coefficient and (b) mean distance to conformity (MDC) values for each phantom image, relative to the average image. These are organized by increasing distance of offset from left to right, as specified in mm distances. The colored bars delineate images into groups based on change in phantom position.

map delivery in real time is quite compelling. The drawbacks of this approach are that the image can be quite noisy and the exact signal quality of this imaging is dependent upon the camera and room lighting conditions. In this study, for simplicity, the room lighting and camera acquisition parameters were all kept fixed for patient imaging and for phantom imaging, to reduce the number of variables studies. However, the camera does online background subtraction as well, so variations in room lights should not have a dominant effect. In the data quality seen, individual frames from the video sequence of Cherenkov images can exhibit low signal-to-noise ratios (typically between 1.5 and 3), but in practice the images are integrated over time such that each video was collapsed to a single image for each control point of the linac. Thus, these summed images provide higher signal-to-noise ratio, which increases with the square root of the number of frames, as would be expected for single photon count statistics. Still, the edge of the beam is where the signal drop off is the most extreme, but this is perhaps also where the utility of the image has the most potential clinical value. Thus, this study was initiated to examine ways to quantify the beam edges

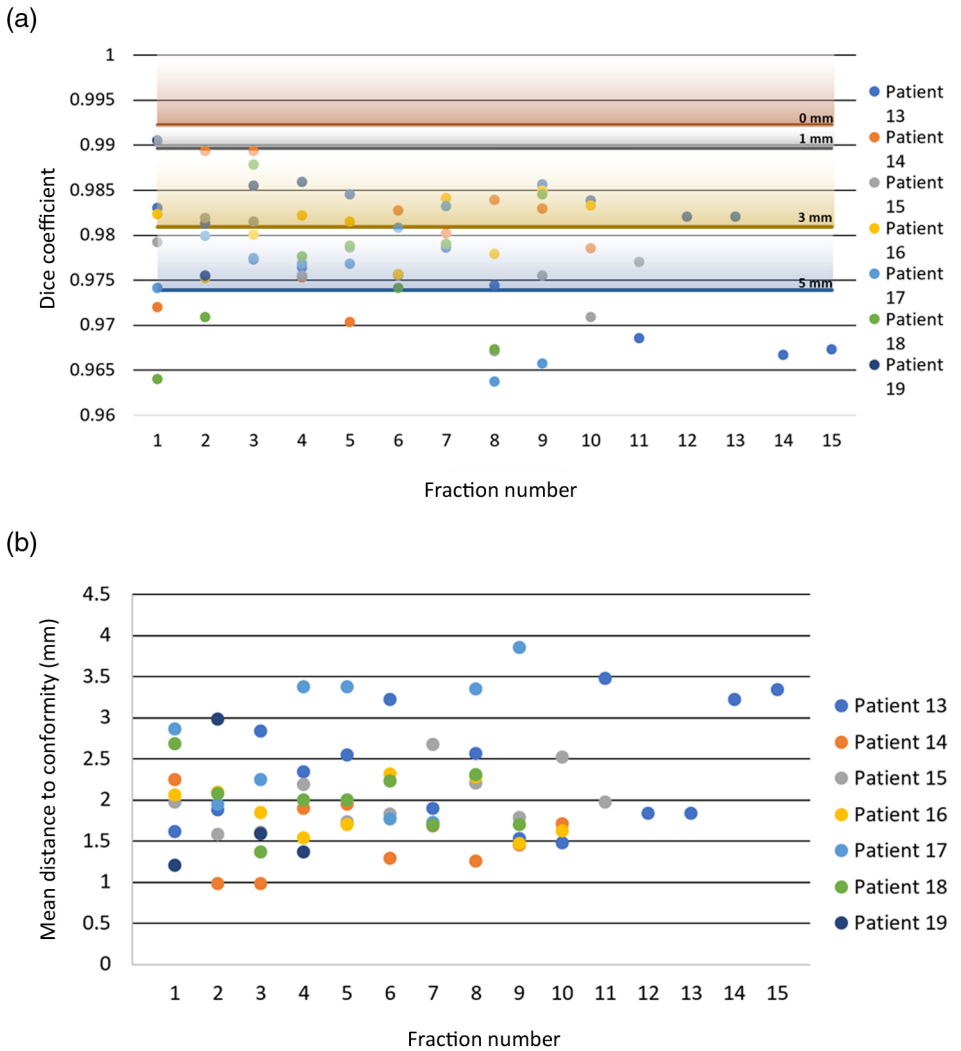

Fig. 7 (a) Dice coefficient and (b) mean distance to conformity are plotted for each patient image. The horizontal lines running across the Dice coefficient versus fraction graph indicate the minimum Dice coefficient from the average of each treatment plan at each distance from the origin.

and examine the utility of day-to-day verification with them, and to specifically test the most logical feature quantification approaches with both phantom and patient data.

The high noise level of these images presents the largest unique challenge when using them for verification of beam edge position on the patient. The beam edge is defined as the point where the beam drops from high Chernekov to near background, and the sharpess of this edge defines how well the edge can be estimated in the thresholding process. At the edges, the intensity data can fall from a few thousand counts down to a few counts, after background subtraction. Given the best-case situation where the detector is shot noise limited, then the signal-to-noise ratio varies as the square root of the signal counts. So the signal-to-noise ratio varied from higher than 10 in the Cherenkov intensity beam field, down to near 1 outside of it. The segmentation algorithms at this noisy border tend to be unreliable, and produce ragged edged segementations, which are dominated by noise variation. As such, preprocessing prior to segmentation is essential, as shown in Fig. 4. After several approaches were tested, the methodology involved a sequence of steps, as is common in most high noise image processing. The final proposed methodology was shown in Fig. 5, which involved (i) denoising the images with a median filter, (ii) thresholding the images into a binary map, (iii) morphologically closing any small holes in the binary image, and (iv) using this map to outline the edge of the beam if needed.

The primary goal of this study was quantitative in nature in terms of using thresholded images and image similarity calculations to objectively determine the segmentation approaches that would be best, based upon matching the expected dose map, as has been shown in a previous study.[11] It is critical to recognize that, as shown in the flowchart of Fig. 2, any small issues in this pipeline of procesing could compromise the observed values of the Dice coefficint or MDC. As such, the systematic testing with breast phantoms and a range of treatment plans was essential to evaulate the expected success of the algorithm, and a range of options was tested before finalizing this processing pipeline.

One expected outcome from the data analysis was that patient data largely have more variation due to reasons other than noise. Patients move in a wide range of directions during daily alignment, and temporal changes during each fraction such as breathing alter the positioning more than the highly titrated movements of the phantoms studied here. Still, the patients in

this study were all aligned by AlignRT (VisionRT, London, United Kingdom)-based positioning, and were expected to be within the 3-mm position verification goal. The observed DICE coefficient values were slightly more variable than the 3-mm phantom position Dice coefficient, likely because of this difference in the complexity of day-to-day positioning. In the phantom study here there were only linear translations in a single direction, whereas patient positioning has a signifcantly more complex set of tanslations and rotations that can occur. Still, the phantom data are well calibrated and so a comparison to this well-known offset data set provides insight into the magnitude of the offsets seen in the patients. The Dice coefficients from the phantom data still provide the absolute measurement of the similarities of two images. Interestingly though, the patient data did not have any observable day-to-day trends in positioning error, as fluctuations in Dice and MDC values appeared to be uniformly scattered across the order of daily fractions. The distortions in real breast tissue are clearly much more complex than the linear offsets produced in the phantoms; however, this comparison was acutally the point of the study. We were able to use the controlled linear offsets to estimate the magnitudes of the variations seen in the patient data, where rotation and distortion would be coupled in with linear offsets. Still the patient offset numbers indicate that they would be consistent with near 3-mm agreement.

It is also prudent to note that the Dice and MDC coefficients were calculated using the average of all treatment days per patient as the "truth" or reference beam shapes for each control point because algorithm development occurred after the full course of treatment was completed. In order for this approach to be viable through the duration of treatment, it will be necessary to determine the appropriate reference image before the treatment dataset is complete. This could take the form of a to-date average Cherenkov binary footprint image, or a simulation beam shape image. Future work aims at using the projected beam shapes delineated by the treatment planning system as the gold standard for beam position verification to eliminate this issue.

5 Conclusions

In this study, the sequence of image processing steps that could maximize the ability to recover the beam edges was analyzed and outlined. The image processing steps chosen were based upon results that had minimal numerical metric difference between comparators of images in unmoved samples and maximal numerical metrics of the moved samples. Because of the particular nature of the noise in the Cherenkov images, the video-rate frames must be processed by integrating the video data into still composite (or time integrated) images at each control point, followed by median filtered denoising, and morphology fixes through small hole removal. These processed images are then transformed into a refined binary mask, from which day-to-day comparisons can be computed, and either the DICE coefficient or the MDC values can be used to analyze them. The patient data from a cohort of subjects imaged in their standard fractionated whole breast radiotherapy were shown to be in good match to a breast phantom imaged in different fractionated radiotherapy treatment plans. The systematic shifts of the phantom approach the expected values of the patient data. Future work with this processing algorithm can be used to analyze the variations seen in patients being treated with concurrent Cherenkov imaging to measure the day-to-day variations in delivery as a quality audit system for patient position and beam verification.

Disclosures

Authors B.W.P., M.J., and V.K. are all employees of DoseOptics LLC, founded to commercialize Cherenkov imaging as a tool in clinical radiotherapy and so have an inherent financial interest in the results of this work. DoseOptics LLC is the recipient of SBIR funding R44 CA199836, which supports some of the research work of P.B., D.J.G., and L.A.J.

Acknowledgments

This work was financially supported by the National Institutes of Health research Grants R44 CA199836 (B.W.P., M.J., P.B., V.K., D.J.G., and L.A.J.) and R01 EB023909 (C.S., B.W.P., I.I.T., J.M.A., D.J.G., and LAJ).

References

1. S. M. Elnahal et al., "Identifying predictive factors for incident reports in patients receiving radiation therapy," *Int. J. Radiat. Oncol. Biol. Phys.* **94**(5), 993–999 (2016).
2. T. Pawlicki, M. Coffey, and M. Milosevic, "Incident learning systems for radiation oncology: development and value at the local, national and international level," *Clin. Oncol.* **29**(9), 562–567 (2017).
3. N. G. Zaorsky et al., "ASTRO APEx(R) and RO-ILS are applicable to medical malpractice in radiation oncology," *Future Oncol.* **12**(22), 2643–2657 (2016).
4. A. Novak et al., "Targeting safety improvements through identification of incident origination and detection in a near-miss incident learning system," *Med. Phys.* **43**(5), 2053–2062 (2016).
5. K. Ricketts et al., "Clinical experience and evaluation of patient treatment verification with a transit dosimeter," *Int. J. Radiat. Oncol. Biol. Phys.* **95**(5), 1513–1519 (2016).
6. L. Cozzi, A. Fogliata, and G. Nicolini, "Pre-treatment verification of intensity modulated photon beams with films and electronic portal imaging–two years of clinical experience," *Zeitschrift für Medizinische Physik* **14**(4), 239–250 (2004).
7. A. Alia, J. Mar, and R. Pastor-Barriuso, "Reliability of portal control procedure in irradiation of breast cancer: a Bayesian analysis," *Radiother. Oncol.* **75**(1), 28–33 (2005).
8. M. Deutsch, J. Bryant, and G. Bass, "Radiotherapy review on national surgical adjuvant breast and bowel project (NSABP) phase III breast cancer clinical trials: is there a need for submission of portal/simulation films?" *Am. J. Clin. Oncol.: Cancer Clin. Trials* **22**(6), 606–608 (1999).
9. L. A. Jarvis et al., "Cherenkov video imaging allows for the first visualization of radiation therapy in real time," *Int. J. Radiat. Oncol. Biol. Phys.* **89**(3), 615–622 (2014).
10. J. M. Andreozzi et al., "Cherenkov imaging method for rapid optimization of clinical treatment geometry in total skin electron beam therapy," *Med. Phys.* **43**(2), 993–1002 (2016).
11. R. Zhang et al., "Cherenkoscopy based patient positioning validation and movement tracking during post-lumpectomy whole breast radiation therapy," *Phys. Med. Biol.* **60**(1), L1 (2015).
12. F. Newman et al., "Visual sensations during megavoltage radiotherapy to the orbit attributable to Cherenkov radiation," *Med. Phys.* **35**(1), 77–80 (2008).
13. A. K. Glaser et al., "Time-gated Cherenkov emission spectroscopy from linear accelerator irradiation of tissue phantoms," *Opt. Lett.* **37**(7), 1193–1195 (2012).
14. J. M. Andreozzi et al., "Camera selection for real-time in vivo radiation treatment verification systems using Cherenkov imaging," *Med. Phys.* **42**(2), 994–1004 (2015).
15. K. N. Chaudhury and S.D. Dabhade, "Fast and provably accurate bilateral filtering," *IEEE Trans. Image Process.* **25**(6), 2519–2528 (2016).

Clare Snyder is currently working toward her BS degree in information science, systems, and technology from the Cornell University College of Engineering with intent to graduate in the spring of

2019. Her research interests include image processing and management science.

Brian W. Pogue is a professor of engineering science and director of MS and PhD programs at the Thayer School of Engineering at Dartmouth, as well as the CAMPEP accredited Medical Physics Education Program at Dartmouth. He is the incoming editor-in-chief of the *Journal of Biomedical Optics* with SPIE Publications, and his research focuses on a range of applications for optics in medicine, with a particular focus on guidance for cancer surgery and radiation therapy.

Michael Jermyn is a researcher at the Thayer School of Engineering at Dartmouth and principal software engineer at DoseOptics LLC. He is an expert in computational solutions for biomedical applications, with experience in machine learning, cancer imaging, medical imaging analysis and visualization, software development, and biomedical engineering.

Irwin Tendler received his BS degree in biological engineering and his master's degree in biomedical engineering from Cornell University in 2016. Currently, he is a combined biomedical engineering and medical physics PhD student at Dartmouth College, Optics in Medicine Laboratory. His research interests are focused on novel biomedical dosimetry device development for use in radiation oncology.

Jacqueline M. Andreozzi received her BS degree in electrical engineering from the University of Central Florida and her master's degree in optics and photonics from the University of Alabama in Huntsville. Currently, she is an NIH predoctoral fellow pursuing a PhD in medical physics from Thayer School of Engineering at Dartmouth College. Her research interests involve clinical radiotherapy quality assurance and dosimetry, particularly utilizing Cherenkov imaging techniques.

Petr Bruza is a researcher at the Thayer School of Engineering at Dartmouth and has developed the first time-gated image intensified CMOS camera for use in radiation therapy dosimetry. His work has centered around camera and system development, technology demonstration, and application specialization in Cherenkov dosimetry and molecular imaging.

Venkat Krishnaswamy is an expert in optical design and has been working at the Thayer School of Engineering since 2012. Since 2014, he has been chief technology officer of DoseOptics LLC, developing commercially viable systems for Cherenkov imaging in radiotherapy.

David J. Gladstone is a professor of medicine at the Geisel School of Medicine at Dartmouth, adjunct professor of engineering at the Thayer School of Engineering at Dartmouth, and chief of clinical physics at Dartmouth-Hitchcock Medical Center. He is the cochair of the radiation shared resource at the Norris Cotton Cancer Center, where significant development and testing of Cherenkov emission detection in humans has taken place.

Lesley A. Jarvis is an assistant professor of medicine in the Geisel School of Medicine at Dartmouth and radiation oncologist at the Dartmouth–Hitchcock Medical Center. Her research focus has been on the translation of novel imaging and sensing technologies into clinical practice, to enhance the accuracy and precision of radiotherapy, and as part of this she pioneered the use of Cherenkov imaging in clinical external beam radiotherapy.